

# Pseudo-continuous resonance enhanced multiphoton ionisation: application to the determination of the hyperfine constants of $^{208}\text{Pb}^{19}\text{F}$

P. Sivakumar , C.P. McRaven , P.M. Rupasinghe , T.Zh. Yang , N.E. Shafer-Ray , Trevor J. Sears & Gregory E. Hall

To cite this article: P. Sivakumar , C.P. McRaven , P.M. Rupasinghe , T.Zh. Yang , N.E. Shafer-Ray , Trevor J. Sears & Gregory E. Hall (2010) Pseudo-continuous resonance enhanced multiphoton ionisation: application to the determination of the hyperfine constants of  $^{208}\text{Pb}^{19}\text{F}$ , Molecular Physics, 108:7-9, 927-935, DOI: [10.1080/00268970903567304](https://doi.org/10.1080/00268970903567304)

To link to this article: <https://doi.org/10.1080/00268970903567304>



Published online: 12 Mar 2010.



Submit your article to this journal [↗](#)



Article views: 87



View related articles [↗](#)



Citing articles: 9 View citing articles [↗](#)

## INVITED ARTICLE

### Pseudo-continuous resonance enhanced multiphoton ionisation: application to the determination of the hyperfine constants of $^{208}\text{Pb}^{19}\text{F}$

P. Sivakumar<sup>a</sup>, C.P. McRaven<sup>a</sup>, P.M. Rupasinghe<sup>a</sup>, T.Zh. Yang<sup>a</sup>, N.E. Shafer-Ray<sup>a\*</sup>, Trevor J. Sears<sup>b</sup> and Gregory E. Hall<sup>b</sup>

<sup>a</sup>Homer L. Dodge Department of Physics and Astronomy, The University of Oklahoma, Norman, OK 73019-2061, USA;  
<sup>b</sup>Chemistry Department, Brookhaven National Laboratory, Upton, NY 11973-5000, USA

(Received 11 November 2009; final version received 11 December 2009)

A highly efficient pseudo continuous resonance enhanced multiphoton ionisation detection scheme is presented that combines the sensitivity of resonance enhanced multiphoton ionisation (REMPI) with high resolution. This detection scheme is employed to obtain the  $A(v'=1) \leftarrow X_1(v=0)$  spectra of  $^{208}\text{Pb}^{19}\text{F}$  with a resolution of 90 MHz. The observed  $^{19}\text{F}$  hyperfine splittings are analysed in terms of effective hyperfine parameters that describe the interaction between the fluorine nuclear spin and that of the unpaired electron in the  $A$  and  $X_1$  states of the molecule.

**Keywords:** REMPI; electron dipole moment; precision spectroscopy; hyperfine constants

#### 1. Introduction

Resonance-enhanced multi-photon ionisation (REMPI) spectroscopy became a useful tool for molecular spectroscopy with the spread of tunable nanosecond dye lasers in the 1970s [1–4]. Numerous subsequent extensions and applications of the basic technique have exploited different combinations of ion counting, photoelectron detection, mass resolution through time-of-flight techniques, and recoil velocity measurements. In the present work, we describe a new variation of the technique that provides a sensitive method for the detection of the absorption of a high resolution, but low power, continuous wave laser and use it to measure hyperfine resolved spectra of  $^{208}\text{Pb}^{19}\text{F}$ .

Typically REMPI is carried out with pulsed laser systems running at a repetition rate of 10–5000 Hz. Ions created from each pulse of laser radiation are collected onto a micro-channel plate detector. Mass selection is achieved by measuring the time between the arrival of the pulse of laser radiation and the arrival of the ion at the detector. This pulsed-detection scenario often is ideally suited to an experimental measurement. For example, in the study of the dynamics of a photodissociation or photo-initiated reaction, the pulse of detection radiation must be timed precisely with respect to the pulse of radiation used to dissociate a molecule. For this case, the experiment is not limited by the repetition rate of the detection laser radiation,

but rather by the time it takes to replenish a fresh sample of gas into an interaction volume.

For other experiments, the pulsed detection scenario is severely limiting. An important example is precision beam spectroscopy that requires the resolution of a continuous wave (cw) laser. For a pulsed ionisation-detected cw absorption measurement, two factors can limit the ionisation signal levels. A purely geometrical upper bound on the duty cycle will be given by the sample transit time across the pulsed beam focal volume, divided by the pulse repetition period. With sufficient power in the pulsed laser, saturation conditions can be achieved in relatively large focal volumes. In this case the effective duty cycle may instead be limited by a second factor: the ratio of the lifetime of the excited state produced by the cw laser relative to the repetition period of the pulsed laser. This ratio varies widely from experiment to experiment. For excitation of the  $A \leftarrow X_1$  transition of PbF with our 10 Hz pulsed laser system, the  $5 \mu\text{s}$  lifetime of the  $A$  state [5] implies an effective ionisation duty cycle of  $1:2 \times 10^4$ . In addition to the obvious drawbacks of such a small duty cycle, experiments driven by short pulses of radiation occurring at low repetition rates may also suffer from large  $1/f$  noise.

Here we report a technique that marries the advantages of REMPI with the narrow resolution of cw excitation. Specifically, we combine narrow bandwidth diode laser radiation with pseudo-continuous

\*Corresponding author. Email: shaferry@physics.ou.edu

laser radiation to enable a *pseudo continuous resonance enhanced ionisation scheme* which we refer to as pc-REMPI. This pseudo-continuous laser radiation is the 76 MHz, 6 ps output of a solid state laser pumped optical parametric oscillator system. We apply this pc-REMPI technique to obtain a high resolution spectra of the  $A^2\Sigma_{1/2}(v'=1) \leftarrow X_1^2\Pi_{1/2}(v=0)$  transition in PbF. This 1–0 band spectra allows us to determine the hyperfine constants that describe the interaction of the  $^{19}\text{F}$  nucleus with the unpaired electron spin in both the  $A$  and  $X_1$  states. Our motivation to develop this technique is to both obtain these spectroscopic constants and to create an ultra-sensitive scheme for the detection of PbF. The PbF molecule may play an important role in the measurement of the electron's electric dipole moment ( $e$ -EDM) [6–9].

The next section describes the experimental technique. Section 3 gives the data analysis in terms of a spin-rotational Hamiltonian. Results are summarised in Section 4.

## 2. Experimental

The experimental set up is located on the campus of the University of Oklahoma and is shown schematically in Figure 1. Ionisation occurs via the double resonant ionisation process  $\text{PbF}^+ \leftarrow D(v''=0) \leftarrow A(v'=1) \leftarrow X_1(v=0)$  [9]. The  $A \leftarrow X_1$  transition is driven with 6 mW of 436 nm radiation produced by an optically isolated (Optics for Research IO-5- $\lambda$ -LP, Figure 1, labelled 1) diode laser (Toptica DL-100, Figure 1, labelled 2). The  $\text{PbF}^+ \leftarrow D(v''=0) \leftarrow A(v'=1)$

ionisation process is driven by 6 ps pulses of 476 nm radiation that occur at a repetition rate of 76 MHz. The 6 ps pulse width is chosen to be less than the measured lifetime of the  $D$  state [9]. The average power of this 476 nm laser radiation is typically 700 mW. This source of radiation is created in the following manner: the 532 nm second harmonic output of a 6 ps, 76 MHz, mode-locked neodymium doped yttrium vanadate (Nd:YVO<sub>4</sub>) laser (HighQLaser, picoTrain Figure 1, labelled 7) is used to pump an optical parametric oscillator (OPO, Angewandte Physik und Elektronik Levante Emerald, Figure 1, labelled 6). The output optics of the Nd:YVO<sub>4</sub> laser are modified in order to gain access to the residual 1064 nm laser radiation. The temperature of the second harmonic generation crystal internal to the Nd:YVO<sub>4</sub> laser system is adjusted to produce 5.5 watts of 532 nm laser radiation (the maximum that can be safely used to pump the OPO) and 2.0 watts of residual 1064 nm laser radiation. The OPO produces approximately 1.5 watts of 864 nm laser radiation which is combined in a lithium triborate crystal (LBO, Red Optronics, Figure 1, labelled 8) with the residual 1064 nm laser radiation in order to create the required 476 nm laser radiation by type II sum-frequency generation.

An effusive beam of PbF molecules is created by heating molten lead to 1000°C (typical) in a MgF<sub>2</sub> nozzle [10]. Molecules created in this way enter into a differentially-pumped detection region through a 1.0 mm skimmer. Molecules that travel into the region of focused laser radiation are state-selectively ionised, creating a  $e^-/\text{PbF}^+$  pair. The electrons created in this

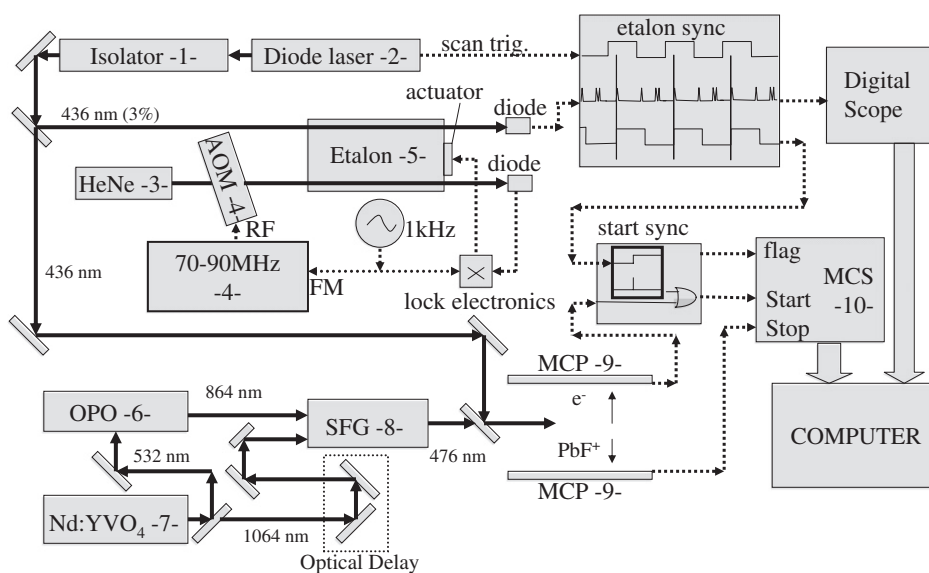


Figure 1. Experimental schematic for our implementation of pc-REMPI. Details are described in the text.

way are accelerated by a uniform electric field to a micro-channel plate detector (Figure 1, labelled 9), and into a timing amplifier (Ortec model 9327) which creates a *start* pulse. The ions are accelerated in the opposite direction to a second micro-channel plate detector, creating a *stop* pulse.

The start and stop pulses are fed into a multi-channel scaler (Ortec model 9353, Figure 1, labelled 10) that logs the events as a function of both the start–stop delay (giving mass resolution) and the time of the start pulse with respect to an internal clock. In principle one could carry out a conventional spectral measurement for which the count rate is measured as a function of a slowly varying diode laser frequency. At the present time, however, we do not have the capability to create such a stable frequency scan. Instead we ramp the diode laser frequency over a range of 4 GHz (typical) and simultaneously monitor the ionisation signal and a calibration signal generated using a cavity stabilised etalon. The manner in which this calibration signal is used to correlate the electron arrival time to the laser frequency is described in the next paragraph.

This internal clock of the multichannel scaler is synchronised to the diode laser frequency sweep by sending synchronisation (sync) pulses to the multi-channel scaler. These sync pulses coincide with the transmission of light through a 1 GHz FSR etalon (Toptica, FPI 100, Figure 1, labelled 5). This etalon is stabilised with a Zeeman stabilised HeNe laser (MicroG LeCoste, ML-1, Figure 1, labelled 3) that is

modulated by an Acousto-Optical device (Newport Electro Optics Systems, N21080-1SAS, Figure 1, labelled 4). A computer is used to accumulate these events as a function of relative frequency and time of flight.

Typical raw data is shown in Figure 2. These data show the  $Q_{fe}$ -branch pile up of the  $A(v'=1, J'=J, f) \leftarrow X_1(v=0, J, e)$  transition. The  $x$ -axis of this plot gives the phase of the start pulse timing with respect to the diode laser scan whereas the  $y$ -axis gives the time of flight (start–stop delay). The spectral plot of Figure 3 is obtained by integrating over a start–stop delay window that isolates the  $^{208}\text{Pb}^{19}\text{F}$  signal and converting the start–stop phase to a frequency shift. By patching together many such scans, we are able to create the spectra of Figure 3. The line width of the spectra shown is 90 MHz. This spectral resolution is not a consequence of the 76 MHz repetition rate of the ionising laser radiation. The diode laser is cylindrically focused onto the molecular beam in a region of space that does not overlap with the ionising laser. With this configuration, it should be possible to obtain a spectral resolution close to the fundamental limit imposed by the lifetime of the  $A$  state. We believe that our current resolution is limited by the combined affects of the spread in beam velocities and divergence of the diode laser radiation. We estimate that the absolute accuracy of this spectra is about 1 GHz, as determined by both by the limited accuracy of our wave meter (Burleigh WA-1000) and our patching technique. The precision

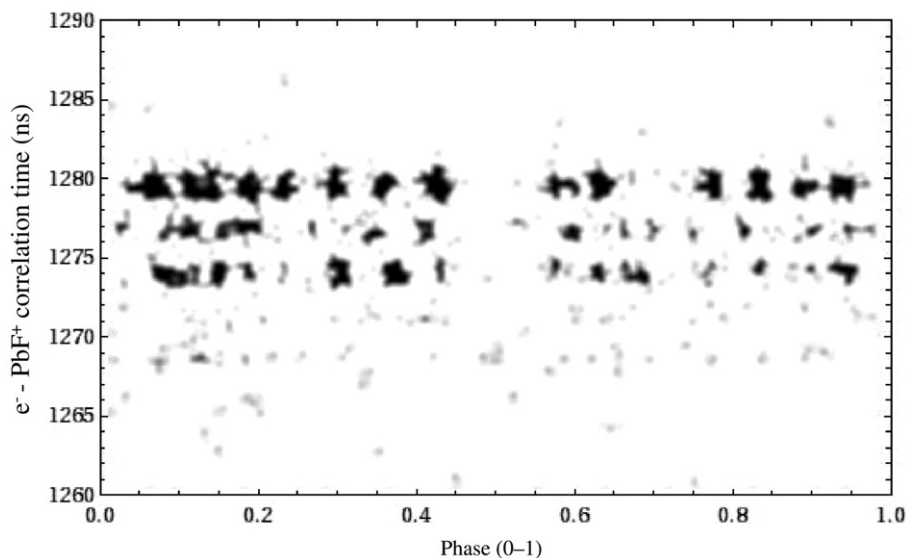


Figure 2. Raw data of the  $Q_{fe}$  branch pile-up of the  $A(v'=1) \leftarrow X_1(v=0)$  transition in  $^{208}\text{Pb}^{19}\text{F}$ . The  $x$ -axis of this plot gives the phase of the start pulse timing as a fraction of the diode laser sawtooth scan time that corresponds to a frequency scan (from blue to red) of approximately 6 GHz. Also visible at shorter  $e^-$ - $\text{PbF}^+$  correlation times are  $X_1 \leftarrow A$  transitions in  $^{207}\text{Pb}^{19}\text{F}$  and  $^{206}\text{Pb}^{19}\text{F}$ . Conversion from phase to frequency is achieved by calibration to a cavity stabilised etalon, as described in the text.

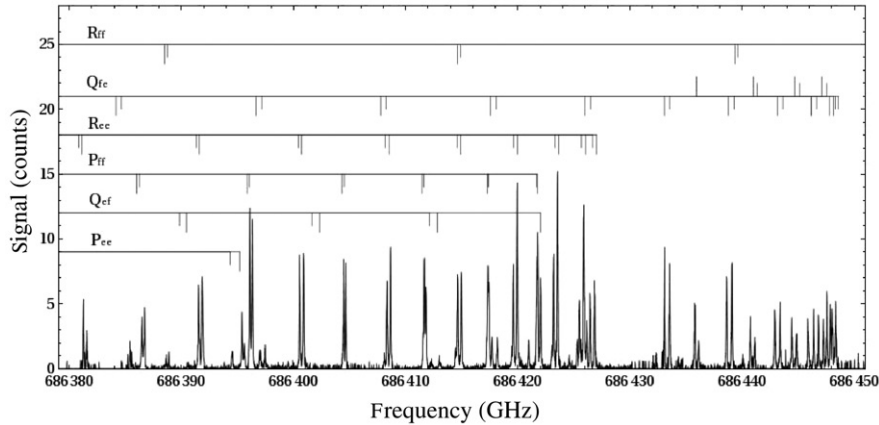


Figure 3. Spectra of the  $A(v' = 1) \leftarrow X_1(v = 0)$  band of  $^{208}\text{Pb}^{19}\text{F}$ .

with which we can measure resolved line splittings is about 10 MHz and is limited by nonlinearity in the scanning mode of the DL100 diode laser.

We note that this scan shows no sensitivity to the high  $J$  lines of the  $R_{ff}$  branch. The absence of these lines does not reflect the rotational temperature of the beam (which we measure in a separate work to be 1000°C [9].) Instead, the lines do not appear because the wavelength of the picosecond laser system is fixed during the scan of Figure 3. By adjusting the wavelength of the pseudo-continuous laser radiation driving the  $D \leftarrow A$  transition, the  $R_{ff}(69/2)$ ,  $R_{ff}(71/2)$ , and  $R_{ff}(73/2)$  can be made to dominate the spectra. We also note that we observe significant line narrowing when Ne is used as a buffer gas instead of He. This suggests that the molecular beam undergoes significant translational cooling, but little or no rotational cooling.

Typical on-resonance  $e^-$ - $\text{PbF}^+$  event rates are 10 to 100 Hz. The introduction of this paper contrasts pc-REMPI with a measurement that employs a cw laser to excite  $\text{PbF}$  molecules to the  $A$  state followed by ionisation produced by radiation from a 10 Hz pulsed laser system (cw + REMPI). It is difficult to access the improvement of pc-REMPI over this cw+REMPI scheme, as attempts to observe  $\text{PbF}^+$  by this second method were unsuccessful. The improvement is expected to be less dramatic than the factor of  $2 \times 10^4$  inferred from the effective duty cycle of the cw + REMPI measurement. The large peak powers of our pulsed laser system allow for a much greater depth of focus and hence a larger probe volume. With this consideration, we estimate an improvement in sensitivity of a factor of  $10^3$ . This leads to an expected collection rate (0.01 to 0.1 Hz) that is consistent with our failure to observe  $\text{PbF}^+$  generated from the cw + REMPI process.

### 3. Determination of the hyperfine constants of $^{208}\text{Pb}^{19}\text{F}$

The rotational spectra of levels of the  $X_1$  and  $A$  states of  $^{208}\text{Pb}^{19}\text{F}$  has been well characterised elsewhere [11–17]. Here we are chiefly concerned with interpreting the hyperfine splitting of each of the rotational transitions we observe. The hyperfine structure of the energy levels of an  $\Omega = 1/2$  molecule are often described in terms of the Frosch and Foley Hamiltonian [18–21]:

$$H_{\text{hfs}} = aI' \cdot L + (b + c)I'_z S_z + \frac{b}{2}(I'_+ S_- + I'_- S_+) + \frac{d}{2} \exp(2i\phi) I'_- S_- + \frac{d}{2} \exp(-2i\phi) I'_+ S_+. \quad (1)$$

If we assume that the valence electron has a wave function of the form

$$\psi_{\pm 1/2} = \sum_{\ell=0}^{\infty} \left[ c_{\ell}^0 |\ell, 0\rangle \left| \pm \frac{1}{2} \right\rangle + c_{\ell}^1 |\ell, \pm 1\rangle \left| \mp \frac{1}{2} \right\rangle \right], \quad (2)$$

then the spectra will be sensitive to the following linear combinations of the Frosch and Foley parameters:

$$A_{\parallel} = \sum_{\ell=0}^{\infty} (|c_{\ell}^0|^2 (b + c) + |c_{\ell}^1|^2 (2a - (b + c))). \quad (3)$$

$$A_{\perp} = \sum_{\ell=0}^{\infty} (a\sqrt{\ell(\ell+1)}(c_{\ell}^{1*} c_{\ell}^0 + c_{\ell}^{0*} c_{\ell}^1) + b|c_{\ell}^0|^2 - d|c_{\ell}^1|^2). \quad (4)$$

These hyperfine parameters are the fine-structure parameters that describe the hyperfine interaction in

terms of an effective spin-rotational Hamiltonian [22,23] with

$$H_{\text{hfs}} = I' \cdot \hat{A} \cdot S' \quad (5)$$

$$= \sum_t (-1)^t A_t I_t' S_{-t}'. \quad (6)$$

The angular momentum operator  $I'$  in Equation (5) acts on the molecular-frame nuclear spin and the angular momentum operator  $S'$  acts on the molecular-frame pseudo-spin  $\Omega$ . The resulting spin-rotational energy is given elsewhere [7,22] and, in the appendix, shown to have the following form:

$$U_{\text{sr}} = U_{\text{rot}} + U_{\text{HF}}, \quad (7)$$

$$U_{\text{rot}} = BJ(J+1) - D[J(J+1)]^2 - q\chi \frac{p}{2} (J + \frac{1}{2}),$$

$$U_{\text{HF}} = -\frac{\chi A_{\perp}}{4} - \frac{q(A_{\parallel} + \chi A_{\perp})}{4(2F+1)} + q \frac{\Delta_{F,\chi}}{2} G \left[ \frac{A_{\parallel} + \chi A_{\perp}}{\Delta_{F,\chi}} \sqrt{\frac{F(F+1)}{(2F+1)^2}} \right] \quad (8)$$

$$\approx -\frac{\chi A_{\perp}}{4} - \frac{q(A_{\parallel} + \chi A_{\perp})}{4(2F+1)}. \quad (9)$$

where  $p_s = \pm 1$  gives the parity with respect to all coordinates except nuclear spin,  $\chi = \pm 1 = (-1)^F p_s$ ,  $q = \pm 1 = 2(J - F)$ , and

$$G[x] = (1 + x^2)^{1/2} - 1, \quad (10)$$

$$\Delta_{F,\chi} = (2F+1) \left( B - \frac{p}{2} \chi - \frac{1}{2} D(2F+1)^2 - \frac{A_{\parallel} + \chi A_{\perp}}{2(2F+1)^2} \right). \quad (11)$$

The approximation of Equation (9) is valid when  $\Delta_{F,\chi} \gg A_{\parallel}, A_{\perp}$ . For our case, the term involving  $\Delta_{F,\chi}$  causes a correction to the ground  $J=1/2$  state energies of about 4 MHz, with the correction rapidly decreasing with increasing  $J$ .

We label each allowed  $A(J', p'_s) \leftarrow X_1(J, p_s)$  transition by  $R_{ee}(J)$ ,  $R_{ff}(J)$ ,  $P_{ee}(J)$ ,  $P_{ff}(J)$ ,  $Q_{ef}(J)$ , or  $Q_{fe}(J)$ . Here  $R$ ,  $P$ , and  $Q$  indicate  $J' = J+1$ ,  $J-1$ , and  $J$  respectively. The first subscript gives the sign of the product  $q'\chi' = p'_s(-1)^{J'-1/2}$  for the  $A$  state, with  $e$  indicating  $q'\chi' = 1$  and  $f$  indicating  $q'\chi' = -1$ . Similarly the second  $e/f$  subscript gives the  $+/-$  sign of the product  $q\chi$  for the  $X_1$  state. For each transition with  $J, J' > 3/2$ , the  $\Delta J = \Delta F$  transitions have a much greater dipole transition strength than the  $\Delta J \neq \Delta F$  transitions and only one hyperfine splitting is observed. The  $J \gg \frac{1}{2}$  limiting form of this splitting, as determined by Equation (8), is given in Table 1.

Whereas  $A_{\perp, X_1}$  and  $A_{\perp, A}$  can be determined from high- $J$  measurements,  $A_{\parallel, X_1}$  and  $A_{\parallel, A}$  are most sensitive to the hyperfine structure of the  $Q(\frac{1}{2})$ ,  $R(\frac{1}{2})$  and  $P(\frac{3}{2})$  transitions. For these transitions, the  $\Delta J = \Delta F$  selection rule breaks, allowing us to observe splittings that depend individually on the energy levels of the  $X_1$  and  $A$  states. For example the difference between the energy  $Q_{ef,11}(\frac{1}{2})$  of the  $A(J' = \frac{1}{2}, e, F' = 1) \leftarrow X_1(J = \frac{1}{2}, f, F = 1)$  transition and the energy  $Q_{ef,01}(\frac{1}{2})$  of the  $A(J' = \frac{1}{2}, e, F' = 0) \leftarrow X_1(J = \frac{1}{2}, f, F = 1)$  is a direct measurement of the  $A(J' = \frac{1}{2}, e, F' = 0, 1)$  level splitting. This splitting is very nearly  $(A_{\parallel, A} + 2A_{\perp, A})/3$  as determined by Equation (9) and indicated in Table 1.

We note that, given our 90 MHz resolution, we are not able to resolve the  $Q_{ef,11}(\frac{1}{2})$  and  $Q_{ef,10}(\frac{1}{2})$  transitions, indicating that the  $F_{X_1} = 0$  and  $F_{X_1} = 1$  hyperfine levels of the ground  $\Omega$  doublet state are very nearly degenerate. We are also unable to resolve the  $Q_{fe,11}(\frac{1}{2})$  and  $Q_{fe,01}(\frac{1}{2})$  transitions, indicating that the  $F'_A = 0$  and

Table 1. Combinations of hyperfine constants used to fit to experimental data.

Parameter	Fit <sup>a</sup> (MHz)	Approximate relation to observation
$\frac{-A_{\perp, A} + A_{\perp, X_1}}{2}$	$-266 \pm 7$	$\Delta R_{ff}(J \gg \frac{1}{2}) = -\Delta R_{ee}(J \gg \frac{1}{2}) = \Delta P_{ff}(J \gg \frac{3}{2}) = -\Delta P_{ee}(J \gg \frac{3}{2})$
$\frac{-A_{\perp, A} - A_{\perp, X_1}}{2}$	$-520 \pm 6$	$\Delta Q_{fe}(J \gg \frac{1}{2}) = -\Delta Q_{ef}(J \gg \frac{1}{2})$
$\frac{A_{\parallel, A} + 2A_{\perp, A}}{3}$	$1070 \pm 10$	$\approx Q_{ef,11}(\frac{1}{2}) - Q_{ef,01}(\frac{1}{2}) = P_{ee,11}(\frac{3}{2}) - P_{ee,01}(\frac{3}{2})$
$\frac{-A_{\parallel, X_1} - 2A_{\perp, X_1}}{3}$	$-300 \pm 20$	$\approx Q_{fe,11}(\frac{1}{2}) - Q_{fe,10}(\frac{1}{2}) = R_{ee,11}(\frac{1}{2}) - R_{ee,10}(\frac{1}{2})$

Note: <sup>a</sup>Errors are only statistical.

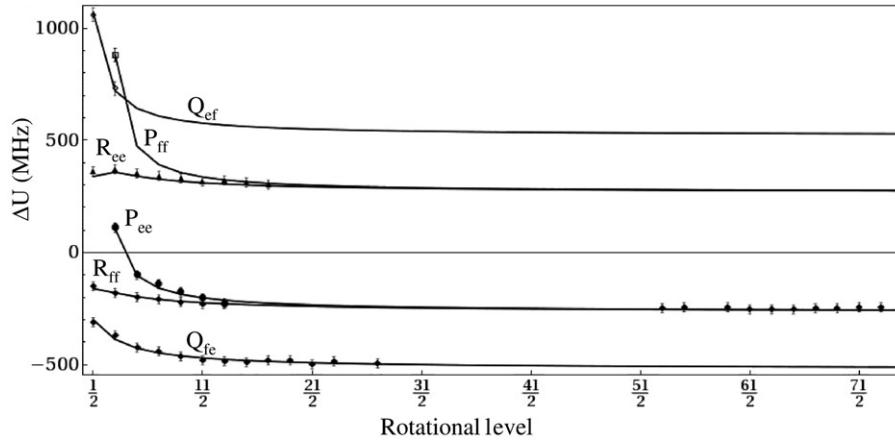


Figure 4. The  $J$ -dependent splitting between the  $A(v' = 1, J', F' = J' + \frac{1}{2}) \leftarrow X_1(v = 0, J, F = J + \frac{1}{2})$  and  $A(v' = 1, J', F' = J' - \frac{1}{2}) \leftarrow X_1(v = 0, J, F = J - \frac{1}{2})$  transitions. The best fit prediction of Equation (8) (solid lines) is compared to experiment (markers).

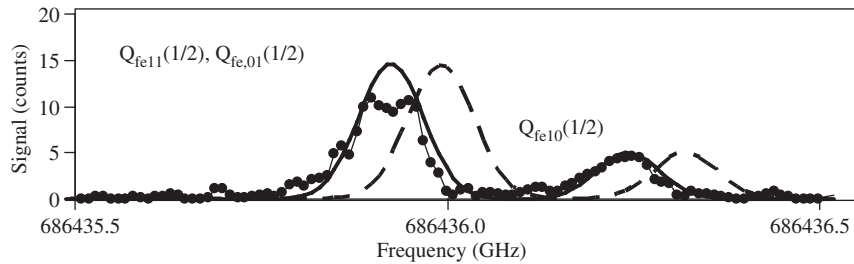


Figure 5. Experimental measurement of the  $Q_{fe}(1/2)$  line profile (filled circles). The solid line gives the expected line shape given the energy distribution of Equation (8) along with a second-order correction for the  $1 \text{ kV cm}^{-1}$  extraction field. The dashed line gives the predicted field-free spectra.

$F'_A = 1$  levels of the upper  $\Omega$  doublet component of the  $J = 1/2$  level of the  $A$  state are very nearly degenerate.

To carry out our analysis, the parameters  $p_{X_1} = -0.1382 \text{ cm}^{-1}$ ,  $B_{X_1} = 0.228027 \text{ cm}^{-1}$  and  $D_{X_1} = 1.852 \times 10^{-7} \text{ cm}^{-1}$  for the  $X_1$  state are taken from Ziebarth *et al.* [15] whereas the parameters  $p_A = 0.6146 \text{ cm}^{-1}$ ,  $B_A = 0.20546 \text{ cm}^{-1}$ ,  $D_A = 2.21 \times 10^{-7} \text{ cm}^{-1}$  for the  $A$  state are taken from Lumley *et al.* [15]. The four combinations of hyperfine parameters appearing in Table 1 are then varied to optimise agreement between experiment and the prediction of Equation (8) for (1) the hyperfine splittings of the  $R_{ee}$ ,  $R_{ff}$  and  $Q_{fe}$  transitions as a function of  $J$  (Figure 4), (2) the line profile of the  $Q_{fe}(1/2)$  hyperfine transitions (Figure 5), (3) the line profile of the  $Q_{ef}(1/2)$  and  $P_{ff}(3/2)$  transitions (Figure 6), and the line profiles of the  $R_{ee}(1/2)$  and  $P_{ff}(1/2)$  transitions (not shown). The resulting values of hyperfine constants, as derived from the data in Table 1, are given in Table 2. A systematic contribution to our error of 2% is due to alignment of

the etalon used for frequency calibration and non-linearity in the diode laser frequency ramp.

We record spectra in an extraction field of  $1 \text{ kV cm}^{-1}$ . For all but the  $J = 1/2$  and  $J = 3/2$  states, this modest field causes no appreciable shift in transition frequencies. Even for these lowest-lying levels, experimental tests show that our measurement of the hyperfine structure individual  $J' \leftarrow J$  transitions is unaffected by the field. The only exception is the  $R_{ee}(1/2)$  transition. At  $1 \text{ kV cm}^{-1}$ , the  $R_{ee,11}(\frac{1}{2}) - R_{ee,10}(\frac{1}{2})$  hyperfine split is measured to be  $305 \pm 5 \text{ MHz}$  (statistical) whereas at  $0.4 \text{ kV cm}^{-1}$  this hyperfine split is measured to be  $290 \pm 5 \text{ MHz}$  (statistical). Likewise the  $R_{ee,22}(\frac{1}{2}) - R_{ee,11}(\frac{1}{2})$  transition shifts from  $385 \pm 5 \text{ MHz}$  at  $1 \text{ kV cm}^{-1}$  to  $365 \pm 5 \text{ MHz}$  at  $0.4 \text{ kV cm}^{-1}$ . Although the hyperfine splitting of individual rotational transitions is small, the field dependent difference in the transition energies between branches is significant. Comparison of our data to a sign-corrected (see acknowledgements) spin-rotational Hamiltonian

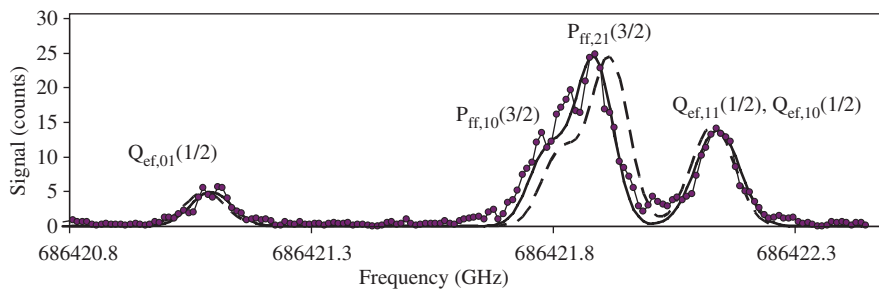


Figure 6. Experimental measurement of the  $Q_{ef}(1/2)$  and  $P_{ff}(3/2)$  line profiles (filled circles). The solid line gives the expected line shape given the energy distribution of Equation (8) along with a second-order correction for the  $1 \text{ kV cm}^{-1}$  extraction field. The dashed line gives the predicted field-free spectra.

Table 2. Measured hyperfine constants with errors that incorporate both statistical and an estimate of systematic contributions.

State	$A_{\perp}$ (MHz)	$A_{\parallel}$ (MHz)
$X_1$	$254 \pm 11$	$392 \pm 63$
A	$785 \pm 18$	$1640 \pm 70$

of Kozlov *et al.* [23] gives the field-dependent distortion of our spectra as shown in Figures 5 and 6. These curves are calculated using the previously predicted dipole moment  $D_{X_1} = 4.62 \text{ D}$  [24]. The spacing of the  $P_{ff}(3/2)$  transitions with respect to the  $Q_{ef}(1/2)$  transitions indicate that  $D_A = 5.5 \pm 0.2 \text{ D}$ ; however this measurement must be regarded as preliminary because it relies on the theoretical prediction of the dipole moment of the  $X_1$  state.

#### 4. Discussion and summary

The observed hyperfine structure of  $^{208}\text{Pb}^{19}\text{F}$  in the  $A^2\Sigma_{1/2}$  and  $X_1^2\Pi$  states can be parameterised by two parameters  $A_{\parallel}$  and  $A_{\perp}$ , or equivalently, by combinations of the Frosch and Foley parameters as given in Equations (3) and (4). For a  $\sigma$  orbital,  $A_{\parallel} = b + c$  and  $A_{\perp} = b$  whereas for a  $\pi$  orbital  $A_{\parallel} = b + c$  and  $A_{\perp} = -d$ . For a heavy molecule like PbF, electronic states tend towards case (c) coupling and mixing of  $\Pi$  and  $\Sigma$  states with the same  $\Omega$  is expected to be severe. The Frosch and Foley parameters can in principle be related to expectation values of the unpaired electron wave function [25], but we lack sufficient information about the partner  $X_2$  state to separate the individual contributions of the  $X_1$  state. We can, however, compare the parameters determined for the ground state of lighter group IV fluorides as shown in Table 3 and see that the current values follow the observed trends. Note that Ge also has a substantial spin orbit

Table 3. Comparison of hyperfine constants of the  $X_1^2\Pi_{1/2}$  state of  $^{208}\text{Pb}^{19}\text{F}$  to those of other ground-state molecules.

Molecule	$A_{\perp}$ (MHz)	$A_{\parallel}$ (MHz)
$\text{CF}^a$	-792	1496
$\text{SiF}^b$	-359	672
$\text{GeF}^c$	-296	620
PbF	$254 \pm 11$	$392 \pm 63$

Derived from data presented in [25] as well as <sup>a</sup>[26], <sup>b</sup>[27], and <sup>c</sup> [28].

coupling and its  $X^2 \Pi_{1/2}$  state will also have a strong tendency towards case (c) behaviour.

For the A state, we can calculate the Fermi-contact parameter  $b_F = b + c/3 = \frac{1}{3}A_{\parallel} + \frac{2}{3}A_{\perp}$  to find  $b_F = 1070 \pm 30 \text{ MHz}$ . This contact parameter measures the spin density at the  $^{19}\text{F}$  nucleus. In a simple molecular orbital picture, this density arises from spin polarisation of the Pb-F sigma bond due to unpaired electron density in the  $6p_{\sigma}$  orbital of the Pb atom.

In summary, we have observed fully state-resolved spectroscopy of the  $A(v' = 1) \leftarrow X_1(v = 0)$  transition in PbF using Pseudo Continuous Resonance Enhanced Multi-Photon Ionisation (pc-REMPE). We have determined hyperfine constants for both the  $X_1$  and A states of  $^{208}\text{Pb}^{19}\text{F}$ . This new pc-REMPE technique has allowed us to marry the advantages of REMPE (mass resolution, high collection efficiency) with 90 MHz resolution possible with excitation by continuous laser radiation. This new technique may play a role in a variety of experiments for which high-sensitivity and high resolution are required, including measurement of the electron's electric dipole moment.

#### Acknowledgements

We acknowledge support of the Department of Energy EPSCoR program (DOE-07ER46361.) Work by GEH and

TJS at Brookhaven National Laboratory was performed under Contract No. DE-AC02-98CH10886 with the US Department of Energy and supported by its Division of Chemical Sciences, Geosciences, & Biosciences. We would also like to thank M.G. Kozlov, A.N. Petrov, and A. Titov. As we were correcting the proofs to this document, these workers brought to our attention a sign error in references 22 and 23 that carried over to reference 10. Their timely intervention prevented this sign error from carrying over to this work as well.

## References

- [1] C.B. Collins, B.W. Johnson, M.Y. Mirza, D. Popescu and I. Popescu, *Phys. Rev. A* **10**, 813 (1974).
- [2] P.M. Johnson, M.R. Berman and D. Zakheim, *J. Chem. Phys.* **62**, 2500 (1975).
- [3] P.M. Johnson, *J. Chem. Phys.* **62**, 4562 (1975).
- [4] D.L. Feldman, R.K. Lengel and R.N. Zare, *Chem. Phys. Lett.* **52**, 413 (1977).
- [5] O. Shestakov, A.M. Pravilov, H. Demes and E.H. Fink, *Chem. Phys.* **165**, 415 (1992).
- [6] N.E. Shafer-Ray, *Phys. Rev. A* **73**, 34102 (2006).
- [7] C.P. McRaven, P. Sivakumar and N.E. Shafer-Ray, *Phys. Rev. A* **78** (5), 54502 (2008).
- [8] M. Rupasinghe and N.E. Shafer-Ray, *Phys. Rev. A* **78** (3), 33427 (2008).
- [9] P. Sivakumar, C.P. McRaven, D. Combs, N.E. Shafer-Ray and V. Ezhov, *Phys. Rev. A* **77**, 62508 (2008).
- [10] C.P. McRaven, P. Sivakumar and N.E. Shafer-Ray, *Phys. Rev. A* **75**, 024502 (2007).
- [11] G.D. Rochester, *Proc. R. Soc. London A* **153**, 407 (1936).
- [12] G.D. Rochester, *Proc. R. Soc. London A* **167**, 567 (1938).
- [13] S.P. Singh, *Indian J. Pure Appl. Phys.* **5**, 292 (1967).
- [14] C.R. Dickson and R.N. Zare, *Opt. Pura Aplic.* **10**, 157 (1977).
- [15] D.J.W. Lumley and R.F. Barrow, *J. Phys. B* **10**, 1537 (1977).
- [16] J. Chen and P.J. Dagdigian, *J. Chem. Phys.* **96**, 1030 (1992).
- [17] K. Ziebarth, K.D. Setzer, O. Shestakov and E.H. Fink, *J. Mol. Spec.* **191**, 108 (1998).
- [18] R.A. Frosch and H.M. Foley, *Phys. Rev.* **88**, 1337 (1952).
- [19] J.T. Hougen, *J. Chem. Phys.* **36**, 2581 (1962).
- [20] I. Kopp and J.T. Hougen, *Can. J. Phys.* **45**, 2581 (1967).
- [21] K. Kawaguchi, S. Saito and E. Hirota, *Mol. Phys.* **55**, 341 (1985).
- [22] M.G. Kozlov, V.I. Fomichev, Y.Y. Dmitriev, L.N. Labzovsky and A.V. Titov, *J. Phys. B: At. Mol. Phys.* **20**, 4939 (1987).
- [23] M.G. Kozlov and L.N. Labzovsky, *J. Phys. B: At. Mol. Opt. Phys.* **28**, 1933 (1995).
- [24] Y.Y. Dmitriev, Y.G. Khait, M.G. Kozlov, L.N. Labzovsky, A.O. Mitrushenkov, A.V. Shtoff and A.V. Titov, *Phys. Lett. A* **167**, 280 (1992).
- [25] J.M. Brown and A. Carrington, *Rotational Spectroscopy of Diatomic Molecules* (Cambridge University Press, Cambridge, 2003).
- [26] S. Saito, Y. Endo, M. Takami and E. Hirota, *J. Chem. Phys.* **78**, 116 (1983).
- [27] M. Tanimoto, S. Saito, Y. Endo and E. Hirota, *J. Mol. Spec.* **100**, 205 (1982).
- [28] M. Tanimoto, S. Saito, Y. Endo and E. Hirota, *J. Mol. Spec.* **116**, 499 (1986).
- [29] R.N. Zare, *Angular Momentum, Understanding Spatial Aspects in Chemistry and Physics* (Wiley Interscience, New York, 1988).

## Appendix 1. Derivation of the hyperfine energy levels of an $\Omega = 1/2$ , $I = 1/2$ molecule

The molecular wave function of the PbF molecule may be written in terms of the symmetric top wave functions of definite parity  $p_s$ :

$$|J, M_J, p_s\rangle = \frac{(2J+1)^{1/2}}{4\pi} \left[ \psi_{1/2} D_{M, \frac{1}{2}}^{J*}(\phi, \theta, \chi) + p_s E^* [\psi_{1/2} D_{M, \frac{1}{2}}^{J*}(\phi, \theta, \chi)] \right], \quad (12)$$

$$= \frac{(2J+1)^{1/2}}{4\pi} \left[ \psi_{1/2} D_{M, \frac{1}{2}}^{J*}(\phi, \theta, \chi) + (i\sigma_y \psi_{1/2}) p_s D_{M, \frac{1}{2}}^J(\pi + \phi, \pi - \theta, \pi - \chi) \right], \quad (13)$$

$$= \frac{(2J+1)^{1/2}}{4\pi} \left[ (\psi_{1/2} D_{M, \frac{1}{2}}^{J*}(\phi, \theta, \chi) + (i\sigma_y \psi_{1/2}) p_s (-1)^{J-1/2} D_{M, -\frac{1}{2}}^J(\phi, \theta, \chi) \right]. \quad (14)$$

Here  $\psi_{1/2}$  is the molecular-frame electronic wave function and the coordinates  $\theta$ ,  $\phi$ , and  $\chi$  give the orientation of the molecular frame. The angle transformation  $\phi \rightarrow \pi + \phi$ ,  $\theta \rightarrow \pi - \theta$ , and  $\chi \rightarrow \pi - \chi$  inverts the molecular-frame  $x$ - $z$  coordinates, (sending the axis of the molecule  $\hat{n}$  to  $-\hat{n}$ ) whereas the reflection  $\sigma_y$  completes the inversion (changing the chirality of the state). If we assume that the valence electron has a wave function given by Equation (2) then

$$i\sigma_y \psi_{1/2} = \sum_{\ell=0}^{\infty} \left[ c_{\ell}^0 |\ell, 0\rangle \left| -\frac{1}{2} \right\rangle + c_{\ell}^1 |\ell, -1\rangle \left| \frac{1}{2} \right\rangle \right] = \psi_{-1/2}, \quad (15)$$

which leads to [25]

$$\left| \Psi_{JM|\Omega}^{p_s} \right\rangle = \frac{\sqrt{(2J+1)}}{4\pi} \left[ \psi_{1/2} D_{M, \frac{1}{2}}^{J*}(\phi, \theta, \chi) + p_s (-1)^{J-1/2} \psi_{-1/2} D_{M, -\frac{1}{2}}^{J*}(\phi, \theta, \chi) \right]. \quad (16)$$

The interaction of an atomic wave function with a nucleus may be written in terms of Frosch and Foley's

hyperfine interaction [18], Equation (1), which we express as

$$H_{\text{hfs}} = \sum_t (-1)^t I_t^1 Q_{-t}^1, \quad (17)$$

$$Q_t^1 = aL_t^1 + (b+c)S_0^1\delta_{t,0} + (bS_t^1 - de^{2it\phi}S_{-t}^1)\delta_{|t|,1}. \quad (18)$$

Here  $I'$  is the nuclear angular momentum in the molecular frame and the rank-1 tensor is given by

$$I_t^1 = \begin{cases} I'_z & \text{for } t=0, \\ \frac{\mp 1}{\sqrt{2}} I'_\pm & \text{for } t=\pm 1. \end{cases} \quad (19)$$

Each value of total angular momentum  $F > 0$  corresponds to four different quantum states corresponding to two values of  $J = F + (q/2)$  (with  $q = \pm 1$ ) and two values of total parity  $\chi = (-1)^F p_s$  (with  $\chi = \pm 1$ ). However, states of opposite total parity can not mix. This implies that the eigen energies can be found by diagonalisation of a two-by-two matrix. To determine this matrix, we first consider the matrix element

$$H_{JI} = \sum_t \langle J' M'_J \Omega' \psi_{\Omega'} | IM'_I | (-1)^t I_t^1 Q_{-t}^1 | JM_J \Omega \psi_{\Omega} | IM_I \rangle \quad (20)$$

$$= \langle J' M'_J \Omega' | IM'_I | D_{st}^1 I_s^1 | JM_J \Omega | IM_I \rangle (-1)^t \langle \psi_{\Omega'} | Q_{-t}^1 | \psi_{\Omega} \rangle. \quad (21)$$

The triple integral over the Wigner rotation matrix can be written as

$$\langle J' M'_J \Omega' | D_{st}^1 | JM_J \Omega \rangle = (-1)^s \langle J' M'_J \Omega' | T_{-s}^1(t) | JM_J \Omega \rangle, \quad (22)$$

where

$$\langle J' \Omega' | T^1(t) | J \Omega \rangle = (-1)^{J+\Omega+1} \sqrt{(2J+1)(2J'+1)} \begin{pmatrix} J' & 1 & J \\ \Omega' & t & -\Omega \end{pmatrix}. \quad (23)$$

We also note that

$$(I' || I^1 || I) = [I(I+1)(2I+1)]^{1/2} \delta_{II'}. \quad (24)$$

so that the hyperfine interaction may be written in terms of a rank-zero tensor:

$$H_{JI} = \sum_s \langle J' M'_J \Omega' | IM'_I | (-1)^s T_{-s}^1(t) I_s^1 | JM_J \Omega | IM_I \rangle (-1)^t \times \langle \psi_{\Omega'} | Q_{\Omega'-\Omega}^1 | \psi_{\Omega} \rangle, \quad (25)$$

which implies (see [29], p. 195.)

$$\begin{aligned} & \langle F' J' IM' \Omega' | H_{\text{hfs}} | F J IM \Omega \rangle \\ &= (-1)^{F+J'+I} \begin{Bmatrix} J & I & F \\ I & J' & 1 \end{Bmatrix} \delta_{MM'} \delta_{FF'} \\ & \times [I(I+1)(2I+1)]^{1/2} [(2J+1)(2J'+1)]^{1/2} \\ & \times (-1)^{J'-\Omega'} \begin{pmatrix} J' & 1 & J \\ \Omega' & \Omega - \Omega' & -\Omega \end{pmatrix} \\ & \times \langle \phi_{\Omega'} | Q_{\Omega'-\Omega}^1 | \phi_{\Omega} \rangle. \end{aligned} \quad (26)$$

Parity considerations require  $\langle \phi_{1/2} | Q_0^1 | \phi_{1/2} \rangle = -\langle \phi_{-1/2} | Q_0^1 | \phi_{-1/2} \rangle$  and  $\langle \phi_{1/2} | Q_1^1 | \phi_{-1/2} \rangle = -\langle \phi_{-1/2} | Q_{-1}^1 | \phi_{1/2} \rangle$ . A connection is made to these matrix elements and the hyperfine constants with

$$A_{||} = 2\langle \phi_{1/2} | Q_0^1 | \phi_{1/2} \rangle = -2\langle \phi_{-1/2} | Q_0^1 | \phi_{-1/2} \rangle, \quad (27)$$

$$A_{\perp} = -\sqrt{2}\langle \phi_{1/2} | Q_1^1 | \phi_{-1/2} \rangle = \sqrt{2}\langle \phi_{-1/2} | Q_{-1}^1 | \phi_{1/2} \rangle. \quad (28)$$

With the substitution  $J = F + (q/2)$  and  $\chi = (-1)^F p_s$  the term  $p_s (-1)^{J-1/2}$  is equal to  $\chi q$ . By substituting this result into Equation (16), one can transform Equation (26) from an  $\Omega$  basis to a total parity  $\chi$  basis. With the addition of the rotational and spin-rotational energies, the complete spin-rotational Hamiltonian for a state of total angular momentum  $F$  and parity  $\chi$  is given by

$$\begin{aligned} & \langle F' q' IM' \chi' | H_{\text{hfs}} + H_{\text{rot}} | F q IM \chi \rangle \\ &= \delta_{FF'} \delta_{MM'} \delta_{\chi\chi'} \left\{ \left( BJ(J+1) - DJ^2(J+1)^2 - \chi q \frac{p}{2} \left( J + \frac{1}{2} \right) \right) \delta_{q,q'} \right. \\ & \quad - \left( \frac{\chi A_{\perp}}{4} + \frac{A_{||} + \chi A_{\perp}}{4(2F+1)} q \right) \delta_{q,q'} \\ & \quad \left. + \frac{A_{||} + \chi A_{\perp}}{2} \left( \frac{\sqrt{F(F+1)}}{2F+1} \right) \delta_{q,-q'} \right\}. \end{aligned} \quad (29)$$

Diagonalisation of this two-by-two matrix leads to the result of Equation (8).